Measurement and Modeling of Both Distant and Close Electric Fields of an M-Component in Rocket-Triggered Lightning

Quanxin Li, Farhad Rachidi, Marcos Rubinstein, Jianguo Wang, Li Cai, Mohammad Azadifar, Amirhossein Mostajabi, Mi Zhou, Yadong Fan

JGR Atmospheres

RESEARCH ARTICLE
10.1029/2019JD032300

Measurement and Modeling of Both Distant and Close Electric Fields of an M-Component in Rocket-Triggered Lightning

Quanxin Li[1,2], Farhad Rachidi[2], Marcos Rubinstein[3], Jianguo Wang[1], Li Cai[1], Mohammad Azadifar[3], Amirhossein Mostajabi[2], Mi Zhou[1], and Yadong Fan[1]

[1]School of Electrical Engineering and Automation, Wuhan University, Wuhan, China, [2]Electromagnetic Compatibility Laboratory, Swiss Federal Institute of Technology (EPFL), Lausanne, Switzerland, [3]University of Applied Sciences of Western Switzerland, Yverdon-les-Bains, Switzerland

Abstract Simultaneous measurements of current and multiple-station electric fields associated with a 5.4-kA-peak M-component in rocket-triggered lightning are presented in this study. A close-range electric field measurement site was located northeast of the triggering site, 195° clockwise from South, at a distance of 78 m, while the distant multiple stations in this study were located southwest of the lightning triggering site (25–48°, clockwise from South) at a distance ranging from 69 to 126 km. Both the fast microsecond-scale and slow millisecond-scale pulses were observed at six distant stations. At the close station, the fast pulse was not noticeable. The magnitude and half-peak width of the fast pulse were in the range of 0.91–1.93 V/m and 2.0–3.0 μs, respectively. The corresponding parameters for the slow pulse were, respectively, in the range of 0.59–1.29 V/m and 20.0–25.1 μs. The time lag between the onset of the channel-base current and the far electric field of the M-component was 18 μs. This time lag was used to deduce the ratio of the M-component channel length and the wave speed. The classical guided wave M-component model proposed by Rakov et al. (1995, https://doi.org/10.1029/95JD01924) to simulate the slow, millisecond-scale field pulse assumes that neither the incident nor the reflected current wave undergoes attenuation even though the wave propagation occurs along a lossy channel. A modified guided wave M-component model is proposed in this study in which the M-component current wave attenuates with an exponential decay. Based on the best agreement achieved between the simulated fields using the modified two-wave M-component model and the observed near and far electric fields, the channel length, the M-component wave speed, and the current attenuation constant were inferred, respectively, as 1.8 km, 1×10^8 m/s, and 3 km. It is shown that the modified guided wave M-component model is able to reproduce reasonably well the electric fields both at close and far distance ranges.

Key Points:
- Both the close (78 m) and six far electric fields (69–126 km) of a 5.4-kA M-component were simultaneously measured in rocket-triggered lightning
- Use is made of the time lag between the onset of the channel-base current and the far electric field of the M-component to infer the value of the ratio of the channel length and the wave speed
- A modified guided-wave M-component model considering the current attenuation as an exponential decay along the channel is proposed

Correspondence to:
F. Rachidi and J. Wang,
farhad.rachidi@epfl.ch;
wjg@whu.edu.cn

Citation:
Li, Q., Rachidi, F., Rubinstein, M., Wang, J., Cai, L., Azadifar, M., et al. (2020). Measurement and modeling of both distant and close electric fields of an M-component in rocket-triggered lightning. *Journal of Geophysical Research: Atmospheres*, *125*, e2019JD032300. https://doi.org/10.1029/2019JD032300

Received 1 JAN 2020
Accepted 4 SEP 2020
Accepted article online 11 SEP 2020

Author Contributions:
Formal analysis: Amirhossein Mostajabi
Investigation: Mi Zhou, Yadong Fan
Methodology: Mohammad Azadifar
Supervision: Jianguo Wang
Writing - original draft: Quanxin Li
Writing – review & editing: Farhad Rachidi, Marcos Rubinstein, Jianguo Wang

1. Introduction

M-components are characterized by a transient increase in the current and the luminosity of lightning channels carrying a continuing current that follows some return strokes (Fisher et al., 1993; Malan & Collens, 1937; Thottappillil et al., 1995, Wang et al., 1999). Experimental data on M-components are available from natural lightning (e.g., Campos et al., 2007; Shao et al., 1995; Stolzenburg et al., 2015; Vayanganie et al., 2014), instrumented towers (e.g., Azadifar et al., 2016; Flache et al., 2008; He, Azadifar, Li, et al., 2018; He, Azadifar, Rachidi, et al., 2018; Miki et al., 2005, 2006; Paul & Heidler, 2018; Pichler & Diendorfer, 2010; Visacro et al., 2013; Zhou et al., 2015), and triggered lightning (e.g., Qie et al., 2011; Rakov et al., 1995, 2001; Tran et al., 2013; Zhang et al., 2017). Only in the latter two cases (instrumented towers and triggered lightning) were the channel-base currents measured simultaneously with the M-component fields. For natural lightning, the current was inferred from remote field measurements.

A guided wave model of M-components was proposed by Rakov et al. (1995) in which the M-component is assumed to be composed of an incident wave, propagating downward along the channel without attenuation, and a reflected wave from the ground that propagates up with the same speed as the downward wave and that vanishes into the cloud when it returns back to the original source. Wang et al. (2007) speculated that an M-component is a composition of many waves occurring at different times and different locations, and those waves may interfere with each other in a complex manner. Jiang et al. (2013) proposed a

modified model considering that the upward wave drains the charge transported by the downward wave. Tran and Rakov (2019) proposed a nonlinear model for the M-component. The fields predicted by their model generally matched measurements better than the classical guided wave model.

As a result of dispersion, the M-component wave is expected to spread while propagating along the channel. Rakov et al. (1995) hypothesized that the ionization produced by the M-component wave front compensates to some extent the dispersion, preserving the more or less symmetrical shape of the current along the channel. The assumption from the classical guided wave M-component model of Rakov et al. (1995) that both, the incident and the reflected current wave, remain unchanged while propagating along the channel (see the Assumption 5 in Rakov et al., 1995) is similar to the transmission line (TL) model in return strokes, and it appears to be inconsistent with propagation along a lossy channel. It has been suggested (e.g., (Karunarathne et al., 2014) that a more realistic model could be similar to the modified TL model (i.e., Modified Transmission Line Model with linear decay [MTLL] and Modified Transmission Line Model with exponential decay [MTLE]), commonly used to simulate the distant electric fields from return strokes.

Jordan et al. (1995) used streak camera records to describe the luminosity evolution along the channel during two M-components of a natural cloud-to-ground (CG) flash. They reported that, as opposed to the return stroke light pulse whose amplitude and waveshape varied markedly with height, the amplitude, and waveshape of one M-component light pulse was essentially invariant with height between the cloud base (about 1 km) and ground. The other M-component described in Jordan et al. (1995) was characterized by a relatively constant light waveshape and a light amplitude that varied somewhat with height.

Wang et al. (2016) investigated three natural CG lightning flashes having both return strokes and M-components. They showed that the total intensity of ionic lines in the spectra (current amplitudes) decreases with the increase of the height along the channel both for the return strokes and for the M-components. However, based on the fact that the total intensity of the spectra is directly proportional to the channel luminance range (apparent diameter) and the fact that the diameter of the channel core is positively related to the longitudinal current (Borovsky, 1988; Wang et al., 2014), they found that the total intensity of the spectra and the apparent diameter for the return stroke decrease as the height increases, while those for M-components at the upper end of the channel are larger (increasing along the channel) than those at the lower end of the channel (see Figures 5–7 in Wang et al., 2016).

Based on the luminosity and current measured at ground for one M-component in rocket-triggered lightning and the Fourier transform of the luminosity waveform, Kotovsky et al. (2019) reported that the luminosity wave exhibited significant dispersion resulting from both the attachment process of the dart leader to the main channel and the propagation through the ionized channel. They noted that, even though it is possible that a significant amount of the wave dispersion occurred during the attachment process, accurate calculations of fields from M-components may need to account for dispersion during wave propagation along the channel.

In this study, simultaneously observed current and associated electric fields at both near and far distances in rocket-triggered lightning are reported, where the fast, microsecond-scale pulse and the slow, millisecond-scale pulse were observed at six far stations. Furthermore, a modified guided wave M-component model considering current attenuation is proposed and tested with the observed close and distant fields.

The proposed modification is aimed at taking into account the effect of channel losses on the M-component current propagation. Losses have already been considered in the model recently proposed by Tran and Rakov (2019) in which the M-component channel was represented as a nonlinear and nonuniform RLCG distributed circuit. The model of Tran and Rakov is more physics-based compared to the model proposed in this paper in which the dispersion effects are ignored. However, Tran and Rakov's model is based on an important number of adjustable parameters, many of which cannot be directly inferred from experimental observations. On the other hand, the number of adjustable parameters in the proposed model is limited to two, and they can be inferred, either directly or indirectly, from experimental observations. The model is also able to reproduce reasonably well the observed electric fields at close and distant ranges.

The paper is organized as follows. Section 2 briefly describes the experimental setup and the instrumentation. Section 3 presents the data set consisting of the simultaneously measured current and multiple-

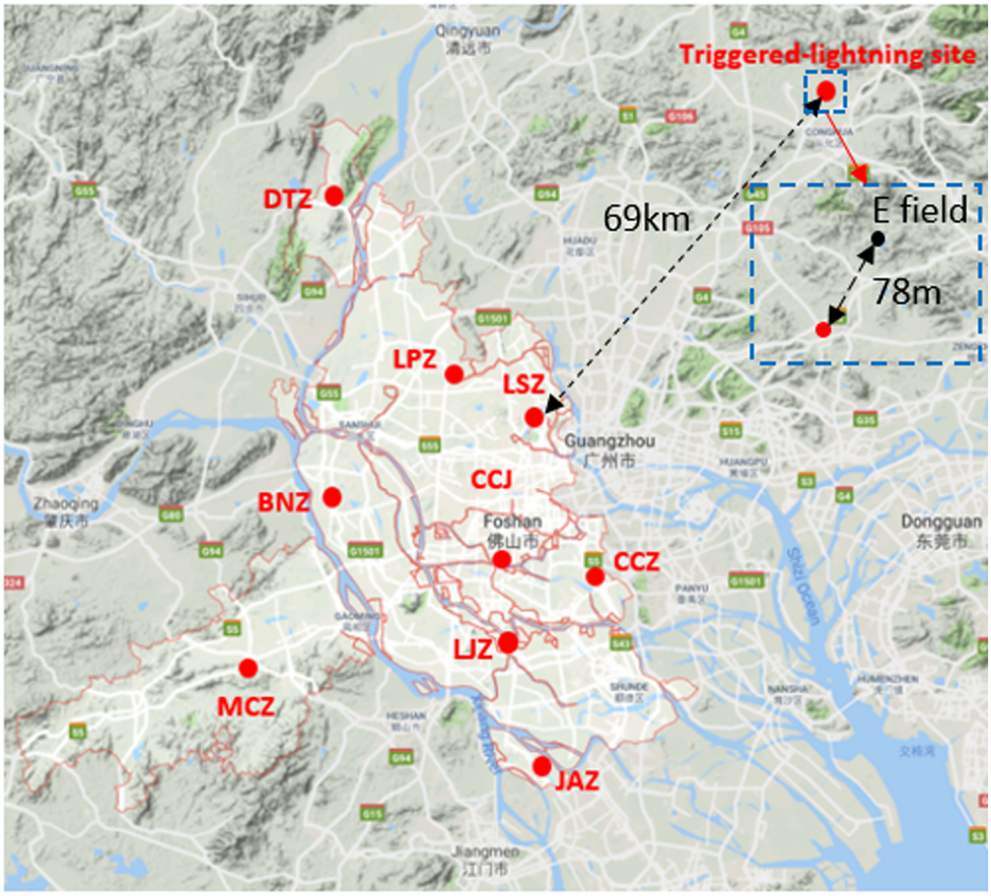

Figure 1. Geographical distribution of the sensors belonging to lightning location system in Foshan (FTLLS), the close electric field, and the observation rocket-triggered lightning site.

station electric fields. Section 4 presents the proposed modification to the classical guided wave model for the M-component. Section 5 presents the results of the comparison between the multiple-station electric field measurements and calculations obtained using the classical and modified models. Finally, general conclusions are given in section 6.

2. Experimental Setup

The triggered lightning site (latitude 23.64°N, longitude 113.59°E), which is located in Conghua, Guangdong, China, started its operation more than a decade ago (e.g., Xiao et al., 2013; Zhang et al., 2014). The lightning current is measured using a 1-mΩ resistive shunt with an overall frequency response of DC to 10 MHz. A fast antenna for the measurement of the vertical electric field is placed at a distance of 78 m in the 15°Northeast direction from the launcher. The frequency response of the fast antenna ranges from 200 Hz to 2 MHz, and its time constant is 2 ms. Both the current waveforms and fast electric fields at close range were digitized by simultaneously using a DL750 oscilloscope at a rate of 10 M Samples/s.

The far electric field sensors belong to the Foshan Lightning Location Systems (FTLLS). The FTLLS has been developed and deployed by Wuhan University, and it started its operation in the summer of 2013 (Cai et al., 2019; Li et al., 2019; Wang et al., 2019). The network contains nine stations shown as red dots in Figure 1 and identified as LSZ, LPZ, DTZ, CCJ, BNZ, CCZ, LJZ, JAZ, and MCZ. The stations are located at distances from the triggered-lightning site of 69, 73, 74, 85, 87, 100, 101, 112, and 126 km, respectively. The triggering site, also shown in Figure 1, is located northeast of the nine sensors. Wideband electric field measuring systems with 3-dB operating frequencies from 160 Hz to 500 kHz and GPS-time synchronization are employed to measure the lightning electric fields at each station. The systems are equipped with analog integrators with a 1-ms decay time constant. The electric field signals produced by triggered lightning

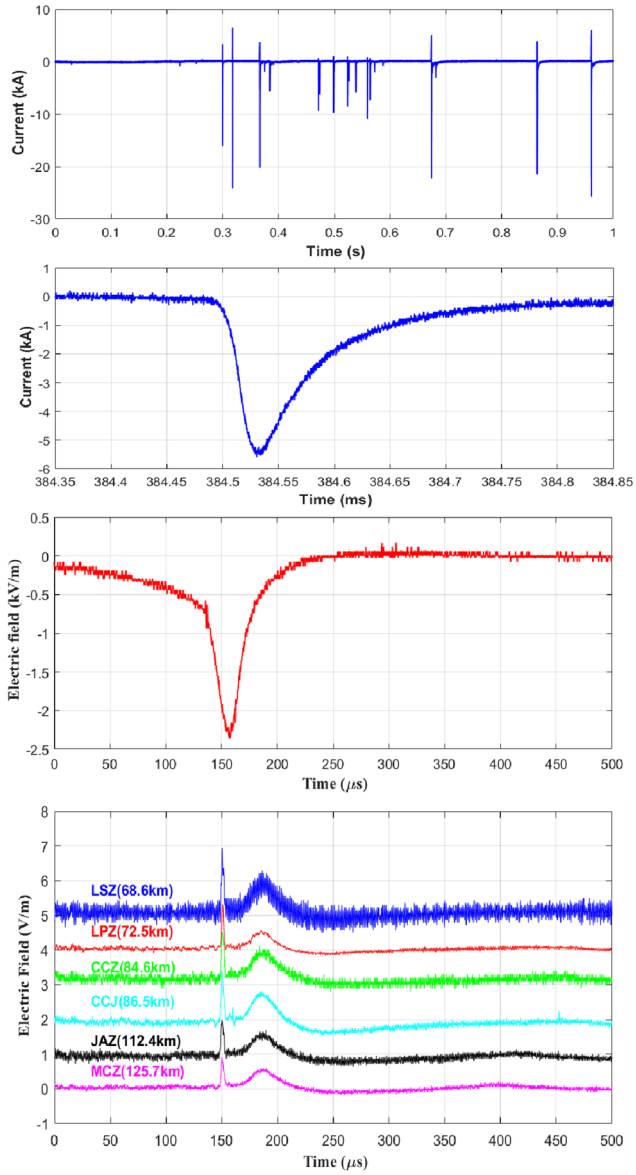

Figure 2. Negative triggered-lightning flash (F20140620) that occurred on 20 June 2014, at 6:43 AM (local time). The flash contained 12 return strokes, more than 30 M-components, of which one M-component was considered in this study. (a) The overall current for the flash. The considered M-component is highlighted in the figure. (b) Expanded view of the M-component current. (c) M-component electric field waveform at 78 m. (d) M-component distant electric field waveform at 69 km.

discharges were digitized with a 10-MS/s sampling rate, 12-bit resolution, and a digital high-speed data-acquisition card. The data recorded by each sensor were transferred optically to the CCJ site, which is the central site of the FTLLS network.

3. Measured Channel-Base Current and Electric Fields

The data set used in this study is composed of simultaneous recordings of currents and multiple-station electric field waveforms of one negative triggered-lightning flash that occurred on 20 June 2014, at 6:43 AM (local time). The flash contained 12 return strokes and more than 30 M-components. One of the M-components was considered in this study. Figure 2a presents the overall current for the flash. The considered M-component is highlighted in the figure. Figure 2b presents an expanded view of the M-component current. The information of the current and field parameters is presented in Table 1. The definition of the parameters is available in Wang et al. (2019). The asymmetrical waveform coefficient (AsWC) of the current waveform has been defined in He, Azadifar, Rachidi, et al. (2018). A fully symmetrical pulse is characterized by an AsWC equal to 1/2, while asymmetrical waveforms characteristic of return strokes or mixed modes have an AsWCs close to 1.0. According to He, Azadifar, Rachidi, et al. (2018), if AsWC for a pulse superimposed on the ICC is lower than 0.8, the pulse can be classified as an M-component-type ICC pulse.

The selected M-component has a particularly high current magnitude. It was selected because it generated fields that could be measured at all the measurement stations. Furthermore, it contained both the slow millisecond-scale field pulse and the preceding fast microsecond-scale pulse, the latter being discernible at all distant measurement stations (69–126 km).

3.1. Fast Microsecond-Scale Pulse and Slow Millisecond-Scale Pulse

The electric field waveform of the M-component at 78 m is shown in Figure 2c. The fast microsecond-scale pulse was not discernible at close distance in the present study, similar to previous studies (e.g., Paul & Heidler, 2018; Rakov et al., 2001; Qie et al., 2011; Zhou et al., 2015).

The distant fields measured at the six distances ranging from 69 to 126 km are shown in Figure 2d. It can be seen in that figure that the electric fields at the distant stations exhibit fast microsecond-scale pulses similar to the junction pulses reported by He, Azadifar, Rachidi, et al. (2018), followed by a slower, millisecond-scale pulse.

Rakov et al. (1992) analyzed the fast microsecond-scale pulses from two data sets in natural flashes in Tampa, Florida, at distances ranging from 2.5 to 12 km and at the Kennedy Space Center with distances from 5 to 27 km. Fast microsecond-scale pulses were observed in 39 (44%) of 88 M-component field changes in Tampa and in 23 (77%) of 30 M-component field changes in KSC. Tran et al. (2013) analyzed 120 M-components in 11 flashes at ICLRT with their electric fields measured at 45 km. They reported that 50% of 76 pronounced M-component current pulses (with magnitudes larger than 165 A) were preceded by microsecond-scale fast pulses. Among the 120 M components, 43 (36%) were preceded by microsecond-scale fast pulses, and the remaining 77 were not preceded by microsecond-scale fast pulses.

Shao et al. (1995) observed the microsecond-scale electric field pulses preceding M-component field changes through the VHF images of the lightning channel and suggested that they were associated with the initiation

Table 1
Salient Parameters of the Measured Current and Electric Fields

		Amplitude (kA)	10–90% risetime (μs)	Asymmetrical waveform coefficient (AsWC)
Current		5.4	29.8	0.72
Close electric field		Amplitude (kV/m)	Half-peak width (μs)	-
Electric field at 78 m		2.33	17.9	-
Far electric fields		Amplitude (V/m)	Half-peak width (μs)	The time lag between the peak point of the fast and slow pulses (μs)
Electric field at LSZ (69 km)	Fast microsecond-scale pulse	1.93	2.2	35.8
	Slow millisecond-scale pulse	1.29	20.0	
Electric field at LPZ (72 km)	Fast microsecond-scale pulse	1.67	2.5	37.2
	Slow millisecond-scale pulse	0.96	20.6	
Electric field at CCZ (84 km)	Fast microsecond-scale pulse	1.42	2.8	37.9
	Slow millisecond-scale pulse	0.91	25.1	
Electric field at CCJ (86 km)	Fast microsecond-scale pulse	1.36	2.0	34.4
	Slow millisecond-scale pulse	0.56	20.5	
Electric field at JAZ (113 km)	Fast microsecond-scale pulse	0.98	3.2	36.3
	Slow millisecond-scale pulse	0.65	20.2	
Electric field at MCZ (126 km)	Fast microsecond-scale pulse	0.91	3.0	36.8
	Slow millisecond-scale pulse	0.59	24.9	

of the M-component charge transfer at the top of the channel to ground. Based on available optical and electric field observations (e.g., Montanyà et al., 2015, Shao et al., 1995), Azadifar et al. (2019) proposed an engineering model in which the microsecond-scale pulse is attributed to the junction of in-cloud leaders and the grounded, current-carrying channel.

Both the fast microsecond-scale pulse and slow millisecond-scale pulse were observed at the six far stations (Figure 2d). As mentioned above, the parameters of the fast and slow pulses from the six stations of the present study are given in Table 1. The magnitude and half-peak width of the fast pulse are in the range of 0.91–1.93 V/m and 2.0–3.0 μs, respectively. Regarding the slow pulse, the corresponding parameters are, respectively, in the range of 0.59–1.29 V/m and 20.0–25.1 μs. The time lag between the peak values of the fast and slow pulses was about 36.4 μs for all the observed distant waveforms.

3.2. The Time Lag Between the Onset of the Channel-Base Current and Electric Fields of M-Components

Figure 3 shows the measured fields and currents for the third return stroke (RS3) in the considered flash. The measured electric fields were recorded at LSZ at 69 km. The time lag between the onset of the M-component channel-base current and the onset of the microsecond-scale electric field, as shown in Figure 3, is 18 μs. The same value was also observed for all other distant observation points. In what follows, we will show that the time lag can be used to deduce the ratio of the M-component channel length (height of the junction point) to the M-component wave speed.

With reference to Figure 4, the distance R from the junction point to an electric field measurement station is given by $D = \sqrt{(d^2 + L^2)}$, where L is the continuing-current-carrying channel height up to the junction point at which the M-component is assumed to have been initiated, and d is the horizontal distance from the base of the channel to the field station. Assuming that the speed of the M-wave as it travels down the channel is v, the time delay (Δt_M) between the onset time of the fast radiated pulse as measured at the measurement station and the onset time of the current at the channel base is $\Delta t_M = \frac{D}{c} - \frac{L}{v_{av}}$. This expression gives the relationship between the channel length L and the average speed of the M-component wave v_{av}, which is defined as follows:

$$v_{av} = \frac{L}{\int_0^L \frac{dz}{v(z)}} \tag{1}$$

in which $v(z)$ is the speed of the M-component wave, which is an arbitrary function of height z.

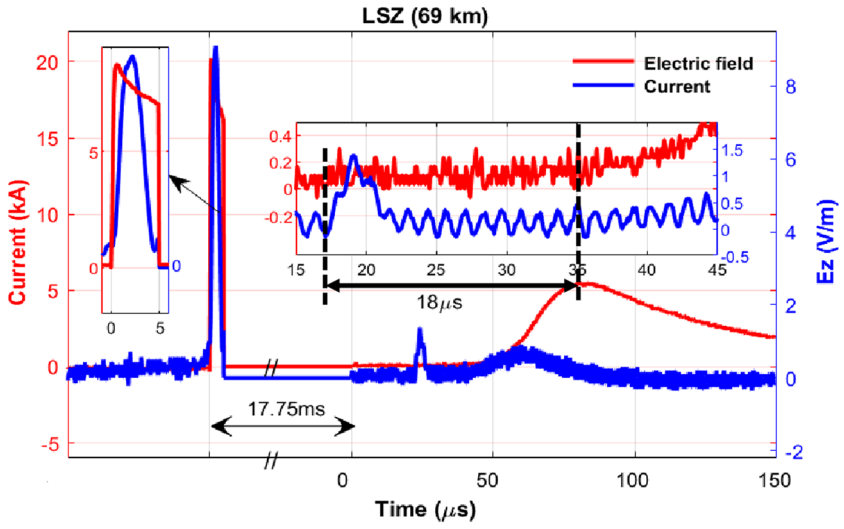

Figure 3. The measured current and its corresponding distant electric field at LSZ (69 km) were aligned through the preceding return stroke (RS3) in flash F20140620 occurred on 20 June 2014, at 6:43 AM (local time).

We will derive a second expression for the relation between those two onset times for the case where the field waveform is time-shifted so that the field and current waveforms of the preceding return stroke are lined up, since that is the technique that we will apply later on in the paper to infer the ratio of the M-component channel length to its wave speed. The time between the preceding return stroke and the time at which its field is measured at the sensor is $\Delta t_{RS} = \frac{d}{c}$.

Figure 4 represents schematically the lightning channel, the return stroke current, and M-component current pulses near the base of the channel. The height of the channel L corresponds to the M-component junction point, namely, the attachment of a newly formed or reactivated branch that gives rise to the M-component. The M-component is assumed to be initiated at a time Δt after the start of the return stroke (t_0). A measurement sensor at a distance d is also shown in the figure. Figure 5 shows the channel-base current and the electric field measured at the observation point at a distance d. If the field in the bottom panel of Figure 5 is shifted by the propagation time d/c to the left, both, the field and the current, can be represented in the same plot as shown in Figure 6.

From Figure 6, the time between the onset of the fast E field that precedes the slow M-component and the onset of the slow M-component current pulse equals the following.

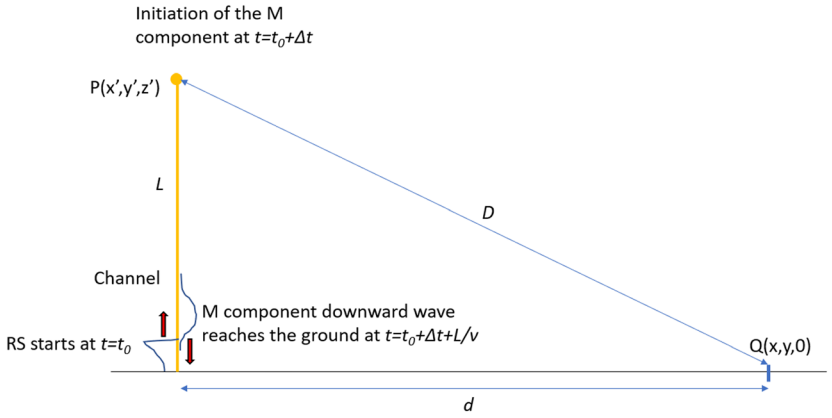

Figure 4. Schematic representation of the lightning channel.

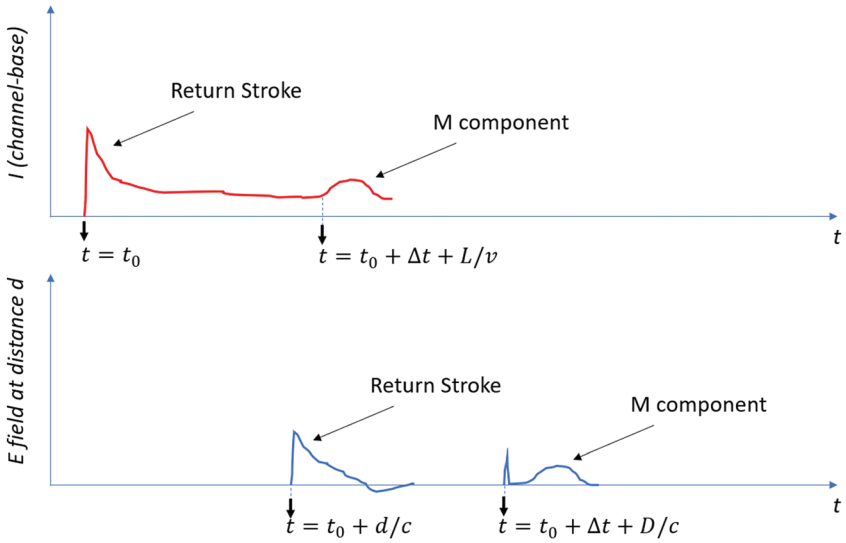

Figure 5. Channel-base current (top panel) and electric field measured at the observation point at a distance d (bottom panel).

$$t_{Fast-Field-To-Slow-Current} = (t_0 + \Delta t + L/v_{av}) - (t_0 + \Delta t + D/c - d/c) = L/v_{av} - D/c + d/c \cong L/v_{av} \quad (2)$$

As in Figure 3, a time shift equal to the propagation time between the channel base and each measurement station was used to line up the return stroke current pulse at the channel base with the corresponding electric field. In addition, the return stroke is assumed to start at time $t = 0$. With reference to the times indicated in the schematic plots of Figure 6, this is equivalent to setting $t_0 = 0$. The onset of the slow current pulse occurs at about 35 μs, while the onset of the fast pulse occurs at about 17 μs. The same values apply for the other measurement stations, even though they are at different distances from the channel. The reason for this is that, as shown in Figure 4, the distance dependence of the time of the onset of the fast pulses is contained in D/c-d/c, which, for the two distances to the measurement stations and for typical values of the length of the channel, is of the order of tens of nanoseconds, and therefore, it is negligible. Therefore, $t_{Fast-Field-To-Slow-Current} = L/v_{av} = 18\mu s$.

4. Modification to the Classical Guided Wave M-Component Model

4.1. The Classical Guided Wave M-Component Model

According to the classical guided-wave model of Rakov et al. (1995), a downward incident current is injected at the top of the continuing-current-carrying channel (injection point or junction height) and travels downward with a speed v. When the incident wave reaches the ground, a reflected wave travels upward at the

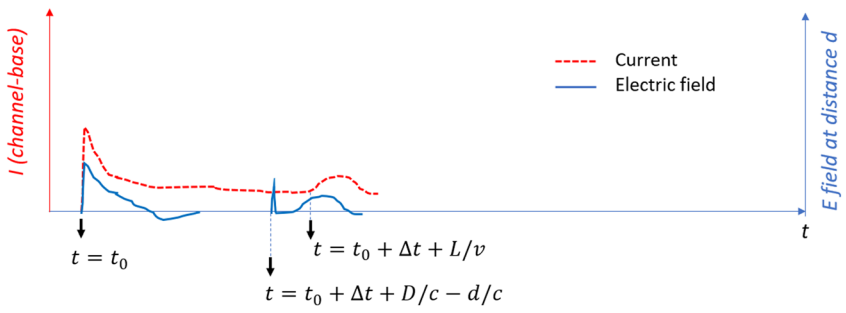

Figure 6. Same as Figure 5, but the field waveform is shifted by the propagation time d/c to the left and superimposed to the current waveform.

speed of the original downward wave. Both the incident downward and reflected upward waves are assumed to travel without suffering attenuation and distortion.

The distribution of the current according to the classical guided-wave model is given by:

$$i(z',t)=\begin{cases} i\left(L,\, t-\dfrac{L-z'}{v}\right), & if \quad t<\dfrac{L}{v} \\ i\left(L,\, t-\dfrac{L-z'}{v}\right)+i\left(L,\, t-\dfrac{L+z'}{v}\right)\rho_g, & if \quad t\geq\dfrac{L}{v} \end{cases} \tag{3}$$

in which v is the velocity of the M-component current wave, assumed to be constant, L is the height of the junction point between the newly formed or reactivated branch and the ICC/CC carrying channel, and ρ_g is the reflection coefficient at the ground. As mentioned in Rakov et al. (1995), a full reflection from the ground ($\rho_g = 1$) can be generally assumed in the model.

4.2. The Modified Guided Wave M-Component Model

In this study, we propose to use a modified version of the M-component guided-wave theory in which the M-component current waves decay exponentially while traveling along the channel, in a similar way as in the MTLE for the return stroke (Nucci et al., 1988; Rachidi & Nucci, 1990). For the sake of generality, to use different decay constants for the downward and upward waves and say that in this work, we assume that both are equal. The distribution of the M-component current along the continuing-current-carrying channel is expressed as follows,

$$i(z',t)=\begin{cases} i\left(L,\, t-\dfrac{L-z'}{v}\right)e^{-\frac{L-z'}{\lambda}}, & if \quad t<\dfrac{L}{v} \\ i\left(L,\, t-\dfrac{L-z'}{v}\right)e^{-\frac{L-z'}{\lambda}}+i\left(L,\, t-\dfrac{L+z'}{v}\right)e^{-\frac{L+z'}{\lambda}}\rho_g, & if \quad t\geq\dfrac{L}{v} \end{cases} \tag{4}$$

where λ is the decay constant of the current. In what follows, we will refer to this model as the modified guided wave model.

4.3. Simulation Parameters and Current Distribution Along the Channel

Figure 7 shows the M-component current distribution along the channel using both the classical guided wave model and the proposed modification. In each figure, we have also presented the contributions of the incident and reflected waves. The computed results correspond to the considered M-component event presented in Figure 2b, as can be seen from the channel-base currents presented in the lower panels, which are the same for both models. The channel-base current is represented analytically using the sum of two Heidler's functions whose parameters were selected to reproduce the measured current waveform, also presented in the lower panels of Figure 7. Reproducing the channel-base current with the proposed model requires the injection of a higher current at the top of the M-component channel compared to the classical guided wave model in which the current does not suffer any attenuation. As a result, the modified two-component guide wave model is characterized by higher incident current waves compared to the classical model (compare the top panel figures). On the other hand, the reflected upward wave at ground level will be the same for the two models. However, the reflected upward wave along the channel for the modified model will have a lower amplitude compared to its counterpart in the classical model as a result of the attenuation.

In the simulations, we have assumed that the reflection coefficient at ground is $\rho_g = 1$. The reason is that the grounding impedance in the rocket-triggered site at Conghua was estimated to be about 5 Ω (Zhang et al., 2014), which is significantly smaller than the channel impedance. The expected propagation speed of the M-wave is estimated to range between 10^7 and 10^8 m/s (page 182, Rakov & Uman, 2003). More detailed information on the measured M-component wave speed is available in the literature (e.g., Jordan et al., 1995; Kotovsky et al., 2019; Malan & Collens, 1937; Malan & Schonland, 1947; Shao et al., 1995; Stolzenburg et al., 2015). The length of the channel was varied from 0.2 to 2.3 km, assuming a constant wave speed of the M-component ranging between 1×10^7 and 1.3×10^8 m/s but keeping always the ratio L/v

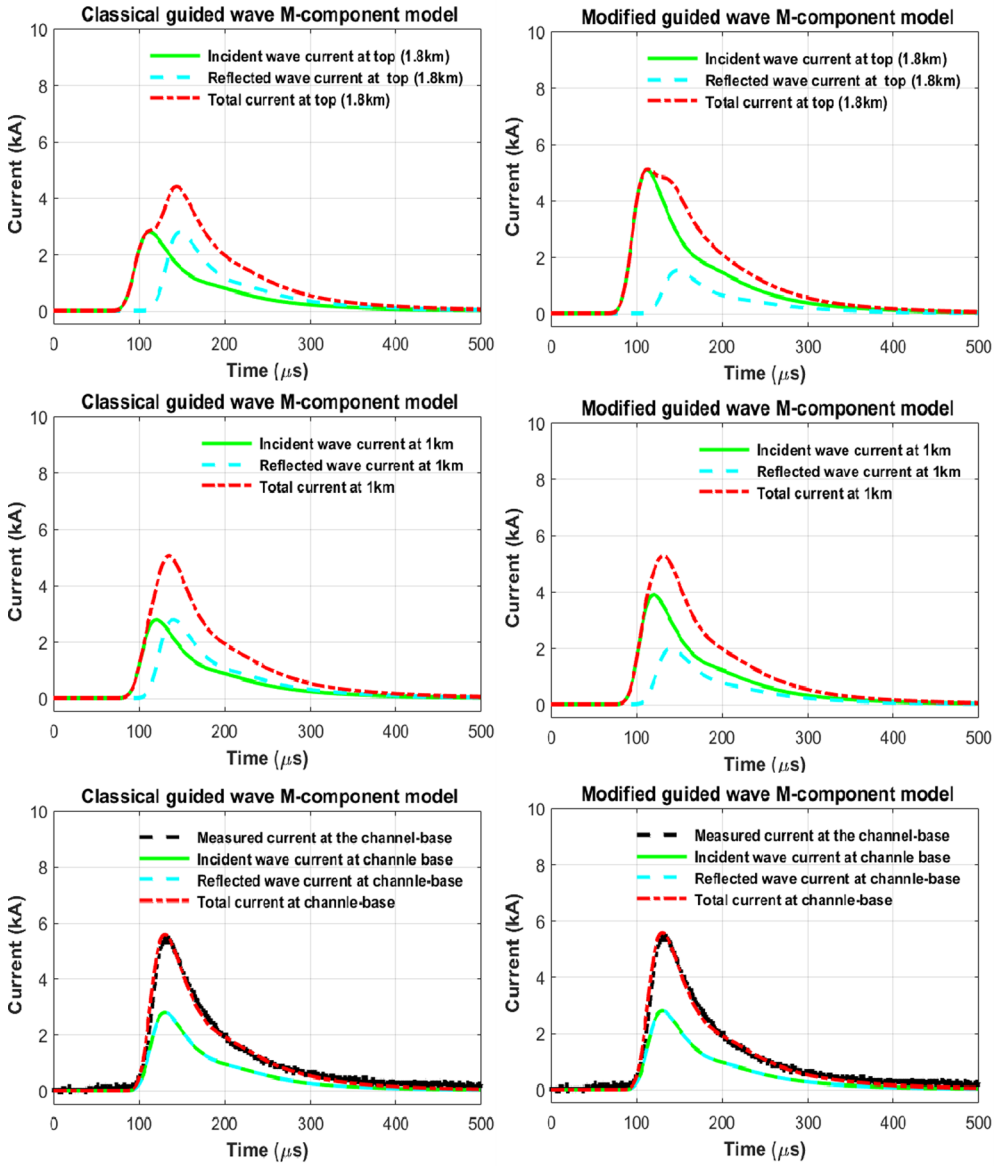

Figure 7. Spatial and temporal current distribution along the channel. Left column: classical guided wave model, right column: modified guided-wave model. Top panel: current at the M-component junction point. Middle panel: M-component current at 1 km. Bottom panel: channel-base current. The considered channel-base current corresponds to the M-component in the flash F20140620, which has been represented analytically using the sum of two Heidler's functions. Modeling parameters: $\rho_g = 1$, $v = 1.0 \times 10^8$ m/s, $L = 1.8$ km. The current decay constant is assumed to be 3 km for the modified model.

constant (18 μs in the present study) and given by equation 4. Finally, the current attenuation constant (λ) used in the modified model was varied from hundreds of meters to 10 km (He, Azadifar, Li, et al., 2018; Nucci & Rachidi, 1989; Rakov et al., 1995). For each model (classical and modified), the parameters that best fit the experimental data were selected, within their considered range and taking into account (4). The inferred parameters for each model are summarized in Table 2.

5. Simulation Results and Comparison With Observed Data

Figure 8 presents the comparison of the measured electric field at 78 m and its corresponding simulation results obtained using the classical guided wave M-component model and the modified model. The model

Table 2
The Inferred Parameters for Each Model

Classical guided wave M-component model		Modified guided wave M-component model	
Reflection coefficient (ρ_g)	1	Reflection coefficient (ρ_g)	1
Wave velocity (v, m/s)	1.0×10^8	Wave velocity (v, m/s)	1.0×10^8
Length of the channel (L, km)	1.8	Length of the channel (L, km)	1.8
		Decay constant of the current (λ, km)	3.0

parameters (Table 2) were selected to best fit the measured data. It can be seen that the measured electric field was reasonably well reproduced by the modified guided wave model. With the classical guided wave model, it was not possible to reproduce the negative unipolar waveshape of the field, regardless of the choice of parameters.

Figure 9 shows the simulated and measured electric fields at far distances, ranging from 69 to 126 km. The same parameters of Table 2 were used for the simulations. Note that the guided wave model and its proposed modification apply only to the slow waveform. The initial microsecond-scale pulse, which is presumably due to the junction process of in-cloud leaders and the current-carrying channel, was recently considered by Azadifar et al. (2019), but it is not considered in our simulations since we are only interested in the slow waveforms. The measured electric fields from of M-components consist of bipolar pulses in a scale of a few hundred microseconds and with superimposed chaotic pulses, clearly visible in the fields of the close station LSZ. These chaotic pulses appear to be consistent with the description of Vayanganie et al. (2014). The microsecond-scale electric field pulses preceding M-component field changes have been attributed to the junction process (Rakov et al., 2001; Shao et al., 1995). It can be seen in Figure 9 that, at distant observation points, the two models perform very similarly, and both are able to reproduce reasonably well the observed waveforms at various distant locations. The modified guided wave M-component model predicts in general slightly larger peak values and faster risetimes compared to the values predicted by the classical model. This can be explained by the larger injected current at the top of the channel and a weaker reflected current along the channel for the modified guided wave M-component model compared to the unattenuated current propagation in the classical guided wave model. The measurement results from the CCJ station show a somewhat smaller amplitude and overshoot compared to the simulated results. The reasons for the observed differences in this station are not known, and they are under investigation. One possible explanation is a calibration problem at that measurement station since other measurements at similar distances do not show that effect.

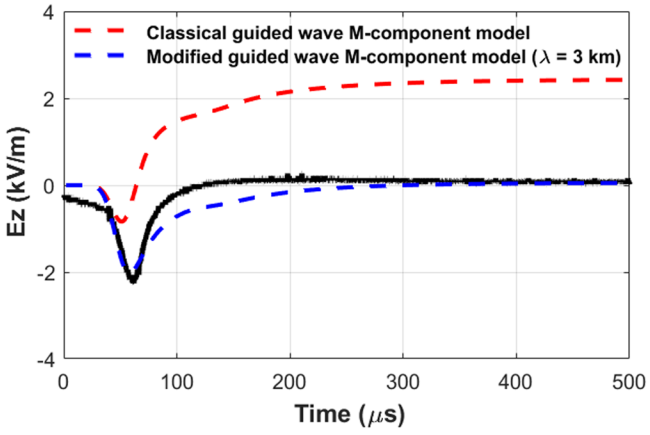

Figure 8. Comparison of the measured M-component electric field at 78 m for flash F20140603 and calculation results using the classical guided wave M-component model (red dashed line) and the modified guided wave M-component model (blue dashed line). $v = 1.0 \times 10^8$ m/s and $L = 1.8$ km. The decay constant was set to 3 km for the modified guided wave M-component model.

Figure 10 shows the influence of the M-component channel height and wave speed on the electric fields. Note that, in agreement with the development presented in section 3.2, the parameters were varied keeping the ratio L/v constant (18 μs in the present study; see equation 4). For the sake of brevity, only the fields at two distances, close (78 m) and distant (69 km), are presented.

Regarding the electric fields at close distance, it can be seen that the classical guided wave M-component model fails in reproducing the late-time response of the field. Specifically, it is not able to reproduce the negative unipolar waveform observed at the considered distance: Regardless of the choice of selected parameters, the resulting field is bipolar. The inability of the classical guided wave model in reproducing the late-time electric field at close distances was already noticed in Rakov et al. (2001). On the other hand, the modified model allows to reproduce the close-distance field early-time and late-time responses with the selected parameters ($L = 1.8$ km and $v = 1 \times 10^8$ m/s). It can be seen that an increase of the M-component wave speed (associated with an increase of the channel height) results in a decrease in the late-time positive overshoot of the field. At the same time, the absolute peak of the initial negative excursion reduces with increasing M-component wave speed.

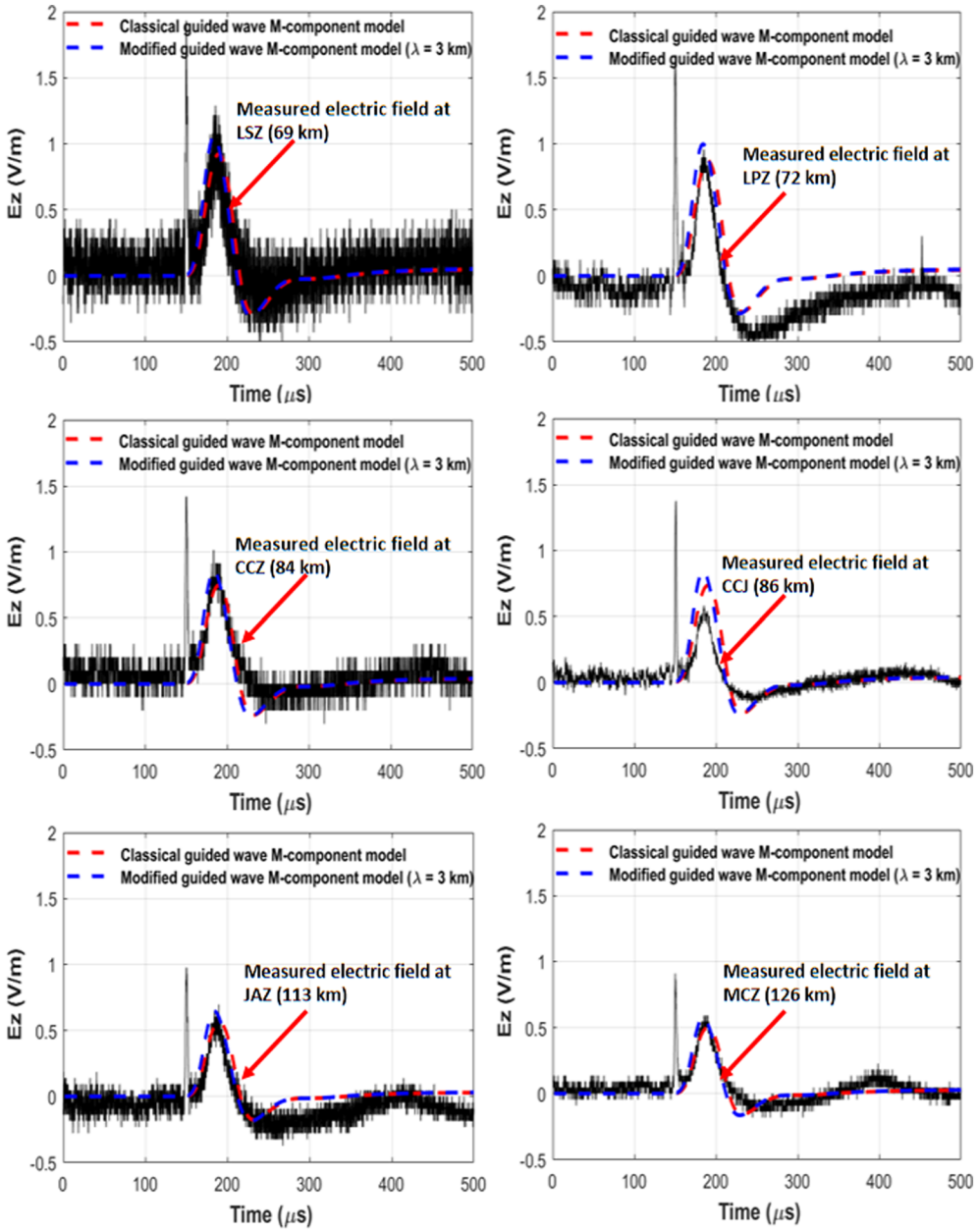

Figure 9. Comparison of the measured M-component electric fields at distant locations (69–126 km) in flash F20140603 and calculation results from the classical guided wave M-component model (red dashed line) and the modified guided wave M-component model (blue dashed line). $v = 1.0 \times 10^8$ m/s and $L = 1.8$ km. The decay constant is set to 3 km for the modified guided wave M-component model.

The lower panels in Figure 10 show the effect of the M-component wave speed (and channel height) on the distant electric field (69 km). It can be seen that an increase in the M-component wave speed would result in an increase of the initial positive field peak as well as an increase of the field negative overshoot.

A discussion is in order on whether the considered pulse corresponds to an M-component or the mixed-mode of charge transfer. The derived length of the channel (junction point height) in the present study is 1.8 km. According to the classification of Zhou et al. (2015), the difference between a classical M-component and a pulse associated with the mixed-mode of charge transfer is essentially the height of the junction point: Relatively low heights correspond to mixed-mode, while higher junction points correspond to M-components. Even though 1.8 km is not a very high junction height, the current and field pulses

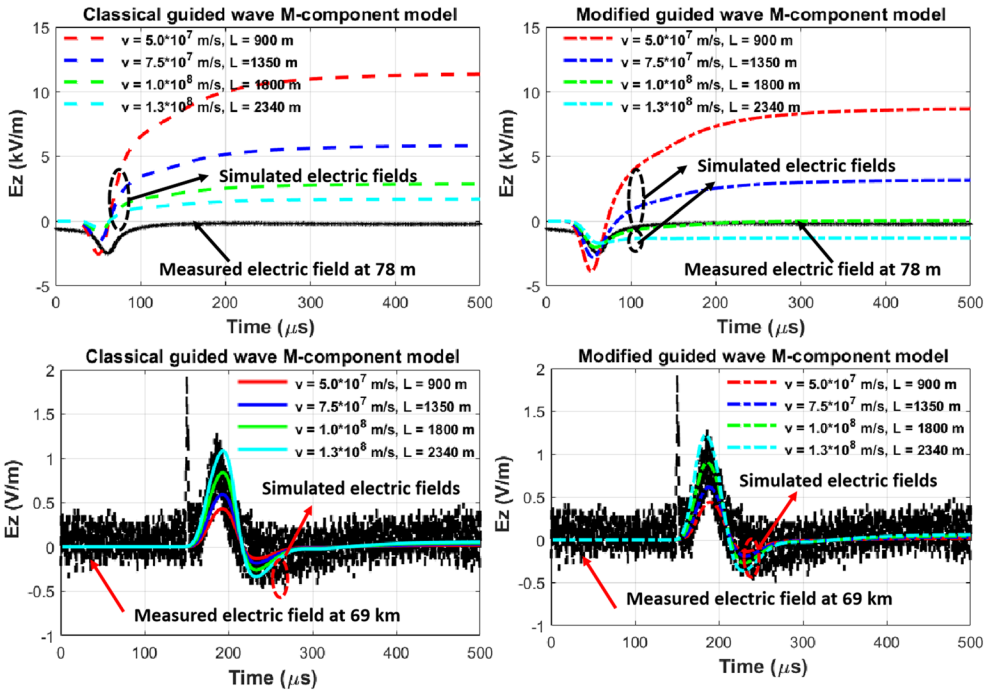

Figure 10. Influence of the M-component channel height and wave speed on the electric fields for the classical guided wave M-component model and modified guided wave M-component model. Decay constant is set to 3 km for the modified guided wave M-component model. Top panel: electric field at 78 m. Bottom panel: electric field at 69 km.

considered in this study correspond to an M-component mode of charge transfer for two reasons: (1) The risetime of the current pulse is 29.8 μs, much longer than the 8-μs criterion proposed by Flache et al. (2008), and (2) the current pulse is characterized by a relatively symmetrical waveshape satisfying the criterion proposed by He, Azadifar, Rachidi, et al. (2018), according to which the so-called AsWC associated with M-components is lower than 0.8, which is the case for the considered pulse in this study for which AsWC is 0.72.

A further point that deserves attention is the ability of the proposed modified guided model to reproduce magnetic fields, which were not recorded in the measurement campaign. Multiple-station magnetic field measurements at Camp Blanding have shown that the M-component magnetic field peaks decay inversely

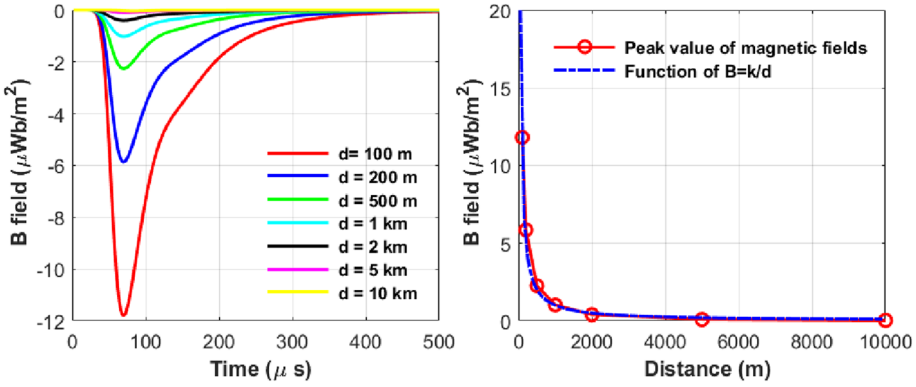

Figure 11. (a) Magnetic induction field as a function of distance using the modified guided wave M-component model. (b) Magnetic induction field peak versus the distance. The considered channel-base current corresponds to the M-component in the flash F20140620, which has been represented analytically using the sum of two Heidler's functions. Modeling parameters: $\rho_g = 1$, $v = 1.0 \times 10^8$ m/s, $L = 1.8$ km. The current decay constant is assumed to be 3 km for the modified model.

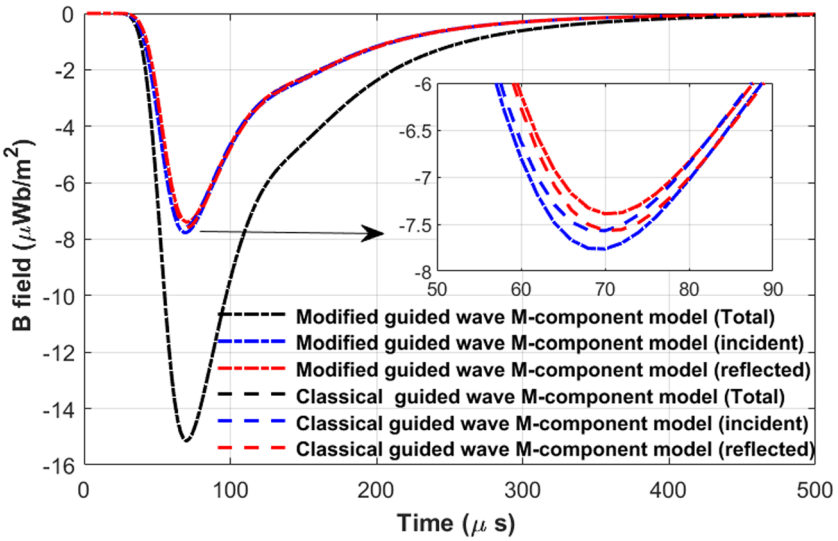

Figure 12. Comparison of the magnetic fields from the modified guided wave M-component model and the classical guided wave M-component model. The considered channel-base current corresponds to the M-component in flash F20140620, which has been represented analytically using the sum of two Heidler's functions. Modeling parameters: $\rho_g = 1$, $v = 1.0 \times 10^8$ m/s, $L = 1.8$ km. The current decay constant is assumed to be 3 km for the modified model. The field is calculated at a distance of 78 m from the lightning channel.

with distance over some hundreds of meters (Rakov et al., 2001). Rakov et al. (2001) also showed that the classical guided wave model is able to reproduce this inverse distance relationship. The magnetic field calculated by the proposed modified model features a similar relationship with distance, in agreement with experimental observations. Figure 11a shows the magnetic induction fields at different distances (100 m–10 km) using the modified guided wave M-component model. Figure 11b shows the plot of the peak magnetic induction field showing an inverse decay with distance.

Figure 12 presents a comparison between the magnetic induction fields calculated using the classical and the modified M-component wave models. The field is calculated at a distance of 78 m from the channel base. For the considered parameters, it can be seen that the magnetic fields predicted by the two models are nearly the same. Of course, for other parameters (for example, longer M-component channel lengths, shorter current risetimes, or faster current decay), more appreciable differences can appear.

The fact that the model was able to reproduce reasonably well the electric fields at close and distant ranges suggests that either the wave dispersion essentially occurs during the attachment process and not while propagating through the ionized channel (Kotovsky et al., 2019), or as hypothesized by Rakov et al. (1995), the dispersion is to some extent compensated by the ionization produced by the M-component wavefront, preserving the current waveshape along the channel.

6. Summary and Conclusions

Simultaneous measurements of current and multiple-station electric fields associated with one M-component belonging to a rocket-triggered lightning flash observed in Conghua, China, were investigated in the present study. The electric field measurements were made at seven different locations, one at close range (78 m) and six at distant ranges (69–126 km). To the best of our knowledge, this is the first experimental set of time-synchronized current and correlated multiple-station electric fields at close and distant ranges associated with M-components.

Both fast microsecond-scale and slow millisecond-scale pulses were observed at six distant stations. At the close station, the fast pulse was not noticeable. The magnitude and half-peak width of the fast pulse were in the range of 0.91–1.93 V/m and 2.0–3.0 μs, respectively. The corresponding parameters for the slow pulse were, respectively, in the range of 0.59–1.29 V/m and 20.0–25.1 μs. The time lag between the onset of the channel-base current and far electric field of the M-component was 18 μs. This time lag was used to infer the ratio of the M-component channel length to the wave speed.

The classical guided wave M-component model proposed by Rakov et al. (1995) to simulate the slow, millisecond-scale field pulse assumes that neither the incident nor the reflected current wave undergoes attenuation even though the wave propagation occurs along a lossy channel. A modified guided wave M-component model was proposed in this study in which the M-component current wave attenuates with an exponential decay. The proposed modification presented in this paper is an engineering approach aimed at taking into account the effect of channel losses on the M-component current propagation. The model ignores dispersion effects, and it uses only two adjustable parameters, namely, the M-component wave speed and the attenuation constant. Based on the best agreement achieved between the simulated fields using the modified two-wave M-component model and the observed near and far electric fields, the channel length, the M-component wave speed, and the current attenuation constant were estimated to be, respectively, 1.8 km, 1×10^8 m/s, and 3 km. While with the classical guided wave model it was not possible to reproduce the negative unipolar waveshape of the field at close distance, the modified guided wave M-component model was able to reproduce this feature. It was also able to reproduce reasonably well the electric fields both at close and far distance ranges.

It is worth noting that, due to the attenuation of the traveling waves as predicted by the modified guided wave model, residual charge will be left on the simulated channel after the M-component process is complete. Notably, this residual charge reduces the long-term electrostatic component of the nearby electric field for the modified model, which is often overestimated in the classical M-component model. It is not unreasonable to conceive that residual charge would be left on the channel that would be later dissipated to ground through conductance or other effects. Note also that the long-term electrostatic field in the classical M-component model results in large part from the charge withdrawn from the top point of the simulated channel. In reality, this charge is likely drawn from broad regions within the cloud. This difference regarding the spatial extent of charge removed during M-events reasonably contributes to the inability of the classical model to effectively model long-term electrostatic field changes. More investigations along with experimental data are needed to draw any definitive conclusions.

Data Availability Statement

This study complies with the AGU data policy. The data are available online (https://zenodo.org/record/4017147#.X1XWonkzY2x, https://doi.org/10.5281/zenodo.4017147).

Acknowledgments

The authors wish to express their gratitude to Prof. Wansheng Dong and Prof. Yijun Zhang from Chinese Academy of Meteorological Science, Beijing, Prof. Shaodong Chen from the Meteorological Bureau of Guangdong Province, and all the members of Guangzhou Field Experiment Site for Triggered Lightning at Conga in Guangdong Province. This work was supported by the National Natural Science Foundation of China (Grant numbers: 51807144 and 51877155), the China Scholarship Council (CSC), the Swiss National Science Foundation (Project No. 200020_175594), and the European Union's Horizon 2020 research and innovation program under Grant Agreement No. 737033-LLR.

References

Azadifar, M., Rachidi, F., Rubinstein, M., Rakov, V. A., Paolone, M., Pavanello, D., & Metz, S. (2016). Fast initial continuous current pulses versus return stroke pulses in tower-initiated lightning. *Journal of Geophysical Research: Atmospheres*, *121*, 6425–6434. https://doi.org/10.1002/2016JD024900

Azadifar, M., Rubinstein, M., Li, Q., Rachidi, F., & Rakov, V. (2019). A new engineering model of lightning M component that reproduces its electric field waveforms at both close and far distances. *Journal of Geophysical Research: Atmospheres*, *124*, 14,008–14,023. https://doi.org/10.1029/2019JD030796

Borovsky, J. E. (1988). Lightning energetics: Estimates of energy dissipation in channels, channel radii, and channel heating risetimes. *Journal of Geophysical Research*, *103*(D10), 11,537–11,553. https://doi.org/10.1029/97JD03230

Cai, L., Zou, X., Wang, J., Li, Q., Zhou, M., & Fan, Y. (2019). The Foshan total lightning location system in China and its initial operation results. *Atmosphere*, *10*(3), 149. https://doi.org/10.3390/atmos10030149

Campos, L. Z. S., Saba, M. M. F., Pinto, O. Jr., & Ballarotti, M. G. (2007). Waveshapes of continuing currents and properties of M-components in natural negative cloud-to-ground lightning from high-speed video observations. *Atmospheric Research*, *84*(4), 302–310. https://doi.org/10.1016/j.atmosres.2006.09.002

Fisher, R. J., Schnetzer, G. H., Thottappillil, R., Rakov, V. A., Uman, M. A., & Goldberg, J. D. (1993). Parameters of triggered-lightning flashes in Florida and Alabama. *Journal of Geophysical Research*, *98*(D12), 22,887–22,902. https://doi.org/10.1029/93JD02293

Flache, D., Rakov, V. A., Heidler, F., Zischank, W., & Thottappillil, R. (2008). Initial-stage pulses in upward lightning: Leader/return stroke versus M-component mode of charge transfer to ground. *Geophysical Research Letters*, *35*, L13812. https://doi.org/10.1029/2008GL034148

He, L., Azadifar, M., Li, Q., Rubinstein, M., Rakov, V. A., Mediano, A., et al. (2018). Modeling of Different Charge Transfer Modes in Upward Flashes Constrained by Simultaneously Measured Currents and Fields, paper presented at IEEE International Symposium on EMC and APEMC, Singapore.

He, L., Azadifar, M., Rachidi, F., Rubinstein, M., Rakov, V. A., Cooray, V., et al. (2018). An analysis of current and electric field pulses associated with upward negative lightning flashes initiated from the Säntis tower. *Journal of Geophysical Research: Atmospheres*, *123*, 4045–4059. https://doi.org/10.1029/2018JD028295

Jiang, R., Qie, X., Yang, J., Wang, C., & Zhao, Y. (2013). Characteristics of M-component in rocket-triggered lightning and a discussion on its mechanism. *Radio Science*, *48*, 597–606. https://doi.org/10.1002/rds.20065

Jordan, D. M., Idone, V. P., Orville, R. E., Rakov, V. A., & Uman, M. A. (1995). Luminosity characteristics of lightning M components. *Journal of Geophysical Research*, *100*(D12), 25,695–25,700. https://doi.org/10.1029/95JD01362

Karunarathne, S., Marshall, T. C., Stolzenburg, M., & Karunarathna, N. (2014). Modeling initial breakdown pulses of CG lightning flashes. *Journal of Geophysical Research: Atmospheres*, *119*, 9003–9019. https://doi.org/10.1002/2014JD021553

Kotovsky, D., Uman, M. A., Wilkes, R. A., & Jordan, D. M. (2019). High-speed video and lightning mapping array observations of in-cloud lightning leaders and an M-component to ground. *Journal of Geophysical Research: Atmospheres*, *124*, 1496–1513. https://doi.org/10.1029/2018JD029506

Li, Q., Wang, J., Rachidi, F., Rubinstein, M., Sunjerga, A., Cai, L., & Zhou, M. (2019). Importance of taking into account the soil stratification in reproducing the late-time features of distant fields radiated by lightning. *IEEE Transactions on Electromagnetic Compatibility*, *61*(3), 935–944. https://doi.org/10.1109/TEMC.2018.2840702

Malan, D. J., & Collens, H. (1937). Progressive lightning. III: The fine structure of return lightning strokes. *Proceedings of the Royal Society of London Series A*, *162*(909), 175–203.

Malan, D. J., & Schonland, B. F. J. (1947). Progressive lightning. VII: Directly-correlated photographic and electrical studies of lightning from near thunderstorms. *Proceedings of the Royal Society of London, Series A*, *191*(1027), 485–503. https://doi.org/10.1098/rspa.1947.0129

Miki, M., Rakov, V. A., Shindo, T., Diendorfer, G., Mair, M., Heidler, F., et al. (2005). Initial stage in lightning initiated from tall objects and in rocket-triggered lightning. *Journal of Geophysical Research*, *110*, D02109. https://doi.org/10.1029/2003JD004474

Miki, M., Shindo, T., Rakov, V. A., Uman, M. A., Diendorfer, G., Mair, M., et al. (2006). Characterization of current pulses superimposed on the continuous current in upward lightning initiated from tall objects and in rocket-triggered lightning. Paper presented at the 28th International Conference on Lightning Protection.

Montanyà, J., van der Velde, O., & Williams, E. R. (2015). The start of lightning: Evidence of bidirectional lightning initiation. *Scientific Reports*, *5*(1), 15180. https://doi.org/10.1038/srep15180

Nucci, C. A., Mazzetti, C., Rachidi, F., & Ianoz, M. (1988). On lightning return stroke models for LEMP calculations. In *19th International Conference on Lightning Protection*.

Nucci, C., & Rachidi, F. (1989). Experimental validation of a modification to the transmission line model for LEMP calculation, 8th Symposium and Technical Exhibition on Electromagnetic Compatibility, Zurich.

Paul, C., & Heidler, F. H. (2018). Properties of three types of M-components and ICC-pulses from currents of negative upward lightning measured at the Peissenberg tower. *IEEE Transactions on Electromagnetic Compatibility*, *60*(6), 1825–1832. https://doi.org/10.1109/TEMC.2018.2802720

Pichler, H., Diendorfer, G., & Mair, M. (2010). Some parameters of correlated current and radiated field pulses from lightning to the Gaisberg tower. *IEEJ Transactions on Electrical and Electronic Engineering*, *5*(1), 8–13. https://doi.org/10.1002/tee.20486

Qie, X., Jiang, R., Wang, C., Yang, J., Wang, J., & Liu, D. (2011). Simultaneously measured current, luminosity, and electric field pulses in a rocket-triggered lightning flash. *Journal of Geophysical Research*, *116*, D10102. https://doi.org/10.1029/2010JD015331

Rachidi, F., & Nucci, C. A. (1990). On the Master, Uman, Lin, Standler and the modified transmission line lightning return stroke current models. *Journal of Geophysical Research*, *95*, 20,389–20,393.

Rakov, V. A., Crawford, D. E., Rambo, K. J., Schnetzer, G. H., Uman, M. A., & Thottappillil, R. (2001). M-component mode of charge transfer to ground in lightning discharges. *Journal of Geophysical Research*, *106*, 22,817–22,831. https://doi.org/10.1029/2000JD000243

Rakov, V. A., Thottappillil, R., & Uman, M. A. (1992). Electric field pulses in K and M changes of lightning ground flashes. *Journal of Geophysical Research*, *97*(D9), 9935–9950. https://doi.org/10.1029/92JD00797

Rakov, V. A., Thottappillil, R., Uman, M. A., & Barker, P. P. (1995). Mechanism of the lightning M-component. *Journal of Geophysical Research*, *100*, 25,701–25,710. https://doi.org/10.1029/95JD01924

Rakov, V., & Uman, M. (2003). *Lightning: Physics and effects*. Cambridge, UK: Cambridge University Press.

Shao, X. M., Krehbiel, P. R., Thomas, R. J., & Rison, W. (1995). Radio interferometric observations of cloud-to-ground lightning phenomena in Florida. *Journal of Geophysical Research*, *100*(D2), 2749. https://doi.org/10.1029/94JD01943

Stolzenburg, M., Marshall, T. C., Karunarathne, S., Karunarathna, N., & Orville, R. E. (2015). An M-component with a concurrent dart leader traveling along different paths during a lightning flash. *Journal of Geophysical Research: Atmospheres*, *120*, 10,267–10,284. https://doi.org/10.1002/2015JD023417

Thottappillil, R., Goldberg, J. D., Rakov, V. A., & Uman, M. A. (1995). Properties of M-components from currents measured at triggered lightning channel base. *Journal of Geophysical Research*, *100*, 25,711–25,720.

Tran, M. D., & Rakov, V. A. (2019). An advanced model of lightning M-component. *Journal of Geophysical Research: Atmospheres*, *124*, 2296–2317. https://doi.org/10.1029/2018JD029604

Tran, M. D., Rakov, V. A., Ngin, T., Gamerota, W. R., Pilkey, J. T., Uman, M. A., & Jordan, D. M. (2013). Microsecond-scale electric field pulses associated with lightning M-components, Abstract AE13B-0356, AGU, Fall Meet.

Vayanganie, S., Cooray, V., Gunasekera, T. A. L. N., Nanayakkara, S., & Fernando, M. (2014). Electric Field Change of M-component, presented at 32rd International Conference on Lightning Protection (ICLP), 1569–1572, China.

Visacro, S., Araujo, L., Guimaraes, M., & Vale, M. H. M. (2013). M-component currents of first return strokes in natural negative cloud-to-ground lightning[J]. *Journal of Geophysical Research: Atmospheres*, *118*, 12,132–12,138. https://doi.org/10.1002/2013JD020026

Wang, J., Li, Q., Cai, L., Zhou, M., Fan, Y., Xiao, J., & Sunjerga, A. (2019). Multiple-station measurements of a return-stroke electric field from rocket-triggered lightning at distances of 68-126 km. *IEEE Transactions on Electromagnetic Compatibility*, *61*(2), 440–448. https://doi.org/10.1109/TEMC.2018.2821193

Wang, D., Rakov, V. A., Uman, M. A., Fernandez, M. I., Rambo, K. J., Schnetzer, G. H., & Fisher, R. J. (1999). Characteristics of the initial stage of negative rocket-triggered lightning. *Journal of Geophysical Research*, *104*, 4213–4222.

Wang, D., Takagi, N., & Watanabe, T. (2007). Observed characteristics of luminous variation events during the initial state of upward positive leaders. *Journal of Atmospheric Electricity*, *7*(1), 61–68.

Wang, X., Yuan, P., Cen, J., Liu, J., & Li, Y. (2014). The channel radius and energy of cloud-to-ground lightning discharge plasma with multiple return strokes. *Physics of Plasmas*, *21*(3), 033503. https://doi.org/10.1063/1.4867381

Wang, X., Yuan, P., Cen, J., & Xue, S. (2016). Correlation between the spectral features and electric field changes for natural lightning return stroke followed by continuing current with M-components. *Journal of Geophysical Research: Atmospheres*, *121*, 8615–8624. https://doi.org/10.1002/2016JD025314

Xiao, T., Zhang, Y., Lu, W., Zheng, D., & Zhang, Y. (2013). Current and electromagnetic field of M-component in triggered lightning. *Journal of Applied Meteorology Science*, *24*(4), 446–454. (in Chinese)

Zhang, Y., Krehbiel, P. R., Zhang, Y., Lu, W., Zheng, D., Xu, L., & Huang, Z. (2017). Observations of the initial stage of a rocket-and-wire-triggered lightning discharge. *Geophysical Research Letters*, *44*, 4332–4340. https://doi.org/10.1002/2017GL072843

Zhang, Y. J., Yang, S. J., Lu, W. T., Zheng, D., Dong, W. S., Li, B., et al. (2014). Experiments of artificially triggered lightning and its application in Conghua, Guangdong, China. *Atmospheric Research*, *117*, 330–343.

Zhou, H., Rakov, V. A., Diendorfer, G., Thottappillil, R., Pichler, H., & Mair, M. (2015). A study of different modes of charge transfer to ground in upward lightning. *Journal of Atmospheric and Solar - Terrestrial Physics*, *125-126*, 38–49. https://doi.org/10.1016/j.jastp.2015.02.008